

## Polyaspartic acid-grafted montmorillonite composite: a new adsorbent for the removal of copper(II), zinc(II), nickel(II)

Dongshen Tong<sup>a,\*</sup>, Min Wan<sup>a</sup>, Youmiao Zheng<sup>b</sup>, Yanrui Han<sup>a</sup>, Jun Hu<sup>a,\*</sup>

<sup>a</sup>State Key Laboratory Breeding Base of Green Chemistry Synthesis Technology, Discipline of Industrial Catalysis, College of Chemical Engineering, Zhejiang University of Technology, Hangzhou 310032, China, Tel. +86 0571 88320062; emails: tds@zjut.edu.cn (D. Tong), hjzjut@zjut.edu.cn (J. Hu), 1597672185@qq.com (M. Wan), 1193381644@qq.com (Y. Han)  
<sup>b</sup>China National Bamboo Research Center, Hangzhou 310012, China, Tel. +86 0571 88869215; email: tong980480@sina.com

Received 1 January 2018; Accepted 21 July 2018

### ABSTRACT

Environment-friendly water treatment has received considerable attention in recent decades. Polyaspartic acid (PASP) is the biodegradable green materials with carboxyl groups (–COOH) and amido groups (–CO–NH–). A new adsorbent, PASP-grafted montmorillonite (Mt) nanocomposite, was prepared and used to remove Cu(II), Zn(II), and Ni(II) ions from aqueous solutions. The synthesized materials were characterized by X-ray diffraction, Fourier transform-infrared spectroscopy, and thermal analysis. The effects of adsorbent amount, pH, initial concentration, and temperature were investigated. The first-order Lagergren model and second-order Lagergren models were used to describe the kinetic data, and the Langmuir, Freundlich, Dubinin–Radushkevich, and Temkin adsorption models were applied to describe the equilibrium isotherms. The results showed the adsorption of Cu(II) onto PASP/Mt is more suitable for Freundlich model, while Zn(II) and Ni(II) ions adsorption belongs to Temkin and Langmuir models, respectively. Second-order model represents the experimental kinetic data in a better manner than first order. In addition, the activation energy, change of Gibbs free energy, enthalpy, and entropy of adsorption were also evaluated for the adsorption. The competitive experiments were also studied to determine adsorptive selectivity of Cu(II), Zn(II), and Ni(II) ions and the selectivity of PASP/Mt for the metals was arranged in follows: Cu(II) > Zn(II) > Ni(II).

*Keywords:* Polyaspartic acid; Montmorillonite; Adsorption; Kinetics; Isotherms

### 1. Introduction

Heavy metal ions are mainly produced by metal-plating facilities, battery manufacturing, metallurgical and electrolytic plating industries. With the rapid development of industries, environmental pollution, especially the heavy-metal pollution, becomes one of the most severe problems [1–6]. Different from organic contaminants, heavy metals are nonbiodegradable and can accumulate, thereby posing great hazard to both human health and environment. An increase of toxic metals in body may cause health problems, such as liver and kidney damage, chronic bronchitis, gastrointestinal

functional disorder, and birth defects [7–11]. So the maximum metal concentration permitted in industrial effluents is strictly controlled by almost all countries in the world. For example, the maximum contaminant level goal for copper is 2.0 mg L<sup>-1</sup> by the World Health Organization. Nowadays, the regulations used to control the concentration of toxic metals in industrial effluents are becoming more and more stringent, as the adverse effects of toxic metals are becoming more well-known. Therefore, toxic metals must be removed from wastewaters in order to protect the environment and living organisms [12,13].

Currently, various methods are used to remove toxic metals, including coprecipitation, ion-exchange, adsorption, membrane separation, electrochemical, and electrodialysis techniques, and so on [14–16]. Among these techniques,

\* Corresponding author.

adsorption is regarded as more appropriate for the removal of toxic metals due to its efficiency and economy [17,18]. Many adsorbents have been studied, such as activated carbon and biological substances, and so on [19,20]. However, due to its high price and regeneration cost, these adsorbents are infeasible as the adsorbent in the future. So the cheaper and more economic adsorbents are still developing underway.

Montmorillonite (Mt) is a kind of layered clay, which is a 2:1-type aluminosilicate [21,22]. They are inexpensive and abundant in nature. In addition, due to its high surface area and cationic exchange capacity (CEC), and chemical stability, they are widely used in many fields including remediation. For its cationic exchange ability, many papers have studied the untreated clay minerals for the heavy metal retention. Several works have been reported on the use of clay minerals as a potential platform for heavy metal retention [23–25]. However, the CEC of the natural clay is not enough and limits its large-scale applications. Because there are many surface broken silanol groups (Si–OH) and layer ending Si–OH groups on the surface of clay, the immobilization of chelating agents on clay minerals has been widely studied for increasing the adsorption capacity [26,27]. From these studies, it was found that two major functional groups are carboxylic group (O-ligand) and amine group (N-ligand), such as malonic acid, citrate, and cysteine, and so on.

Polyaspartic acid (PASP), which has a protein-like amide linkage with carboxyl groups (–COOH) and amido groups (–CO–NH–), is known to be the biodegradable polymeric materials and is widely used in medical, cosmetic, fabric, and metal absorbent materials [28,29]. However, because PASP is water-soluble, they are difficult to collect and reuse if they are directly used. Several works have reported to the preparation of superabsorbent polymeric gels, such as polyacrylamide/attapulgite composite and PASP/palygorskite clay [30,31]. PASP-based superabsorbent is a kind of biodegradable and recyclable material and has been used in agriculture, horticulture, and wastewater treatment.

Therefore, in this investigation, PASP-grafted montmorillonite composite was prepared and the performance for the adsorption of Cu(II), Zn(II), and Ni(II) ions was also evaluated. To the best of our knowledge, it is the first time to synthesize PASP/Mt composites and be used for adsorption. Chemical modification through the process of grafting PASP on the surface of montmorillonite would not only overcome the water-solubility of PASP, but also increase the adsorption capacity of montmorillonite. In addition, PASP is biodegradable green materials and Mt is abundant in nature. So, the novel absorbent is inexpensive and environment-friendly materials, and it may be the alternative substitute to the more costly adsorbents.

## 2. Experimental

### 2.1. Materials

Ca-Mt powder was purchased from Zhejiang Changan Rengheng Science and Technology Co., Ltd., China. The CEC of Mt was 80 meq per 100 g. The silane coupling agent, 3-aminopropyltriethoxysilane (KH-550), obtained from Aladdin Co., Ltd., Shanghai, China. Sodium hydroxide, hydrochloric

acid, and other reagents used in this work were all analytical reagent.

### 2.2. Preparation of amino-Mt

0.04 mol (10 mL) of silane coupling agent KH-550 was dispersed into 40 mL mixed solution of alcohol and deionized water with the volume ratio of 1:1, the volume fraction of mixed solution obtained was 20%. Then 2.0 g of raw Mt was added into the solution under stirring. The mixture was sonicated for 10 min and then stirred at 60°C for 5 h. The product was filtered and washed several times by absolute ethanol and distilled water, and then dried at 80°C for 12 h. The final products were ground to 80–120 mesh.

### 2.3. Preparation of polysuccinimide and PASP

9.8 g (0.1 mol) of maleic anhydride was dissolved in a three-neck flask and 10 mL of ammonia (0.12 mol NH<sub>3</sub>) was slowly added into it under ice water, and then reacted at 85°C for 2 h with magnetic stirring. Finally, the solution was dried at 80°C and polysuccinimide (PSI) was obtained by heating at 220°C for 3 h under nitrogen.

Sodium hydroxide solution (2 M) was added to the suspension of PSI, the mixture was then stirred at 40°C for 40 min under pH = 9. The solution was adjusted to pH = 7.0 with HCl (0.5 M) solution and then filtered, washed with absolute alcohol, and dried at 85°C. Finally the product was ground and PASP was obtained.

### 2.4. Preparation of PASP/Mt

2 g of PSI was dissolved in 20 mL *N,N*-dimethylformamide solution. Then 4 g of amino-Mt was added and stirred at 35°C for 4 h. After the reaction, absolute alcohol was added to the solution and then centrifuged, washed with distilled water. Lastly, the product was dispersed into 10 mL mixed solution of alcohol and distilled water with a volume ratio of 1:1. At the same time, the reaction solution was adjusted to pH = 9.0 using 2.0 M NaOH solution and stirred at 40°C for 40 min. Then the solution was centrifuged, washed, and dried at 85°C for 2 h. Finally the product was ground and PASP/Mt was attained.

### 2.5. Adsorption experiments

Adsorption kinetics and isotherm experiments for metal ions were undertaken in a batch equilibrium technique. The pH experiments were carried out by a 100 mL of 20 mg L<sup>-3</sup> Cu(II), Zn(II) solution with 0.2 g of PASP/Mt and a 100 mL of 40 mg L<sup>-3</sup> Ni(II) solution with 0.6 g of PASP/Mt and the pH was adjusted between 1 and 7 with adding a small amount of 0.1 mol L<sup>-1</sup> HCl or 0.1 mol L<sup>-1</sup> NaOH. The optimum pH was then determined and used throughout all adsorption experiments, which were conducted at various time intervals, the initial concentrations (20–80 mg L<sup>-3</sup>) of Cu(II), Zn(II) solution and 40–100 mg L<sup>-3</sup> of Ni(II) solution) and temperatures (20°C, 30°C, 40°C, and 50°C), to determine the adsorption equilibrium time and the maximum removal of dye. The concentration of metal ions left in the supernatant solution was determined from the calibration curve prepared

by measuring the absorbance of different predetermined concentrations. The concentrations of Cu(II), Zn(II), and Ni(II) ions were measured by a Shimadzu UV-2550 UV-Vis spectrophotometer using wavelengths at 440, 535, and 530 nm, respectively.

The adsorption capacity of a metal ion can be calculated by the equation as follows:

$$Q_e = (C_0 - C_e) \frac{V}{M} \quad (1)$$

where  $Q_e$  is the amounts of metal ions adsorbed at equilibrium adsorption capacity of absorbent ( $\text{mg g}^{-1}$ ),  $C_0$  and  $C_e$  are the initial and equilibrium concentrations of metal ions in the solution ( $\text{mg L}^{-1}$ ),  $V$  is the volume of metal ions solution (L), and  $M$  is the mass of absorbent (g).

## 2.6. Material characterization

The X-ray diffraction (XRD) measurements were collected using a Thermo ARL SCINTAG X'TRA diffractometer between  $2^\circ$  and  $80^\circ$  ( $2\theta$ ) with a scanning rate of  $0.1^\circ \text{ s}^{-1}$ , employing Cu K $\alpha$  radiation ( $\lambda = 1.54056 \text{ \AA}$ ). The nature of surface species was determined by the Fourier transform-infrared spectroscopy (FTIR). The FTIR spectra were registered using a Nicolet AVATAR-370 spectrometer in KBr pellets. The samples were dried at  $110^\circ\text{C}$ , mixed with KBr and exposed to infrared light. The pellets were immediately measured after preparation under ambient conditions in the mid-infrared area. The spectra were the result of averaging 32 scans in wavelengths ranging from  $4,000$  to  $400 \text{ cm}^{-1}$ . Thermal analyses (TG) up to  $800^\circ\text{C}$  were carried out in a NETZSCH STA 449 C using a heating rate of  $10^\circ\text{C min}^{-1}$  with a nitrogen flow rate of  $100 \text{ mL min}^{-1}$ .

## 3. Results and discussion

### 3.1. XRD, FTIR, and thermal analysis

Fig. 1 shows the XRD patterns of PASP, Mt, amino-Mt, and PASP/Mt. The XRD pattern of Ca-Mt showed a main reflection at approximately  $2\theta$  of  $5.65^\circ$ , which agrees with the (001) reflection of Ca-montmorillonite and the basal spacing of  $1.56 \text{ nm}$ . The diffraction peak at  $21.84^\circ$  is related to the presence of opal-CT impurities (such as quartz and calcite) [32,33]. The amino-Mt and PASP/Mt composites showed the similar diffraction peaks to that of Mt, presenting that the layered structure of Mt wasn't destroyed after the modification of PASP. Moreover, the basal spacing of amino-Mt almost unchanged, while the basal spacing of PASP/Mt was a little increased in comparison with Mt, which should be ascribed to the intercalation of PASP into the interlayer of Mt.

The FTIR spectra of PASP, Mt, and PASP/Mt are shown in Fig. 2. According to Fig. 2, two absorption peaks around  $3,430$  and  $3,630 \text{ cm}^{-1}$  could be seen from Mt, which is attributed to stretching vibration of the OH groups and bending vibration at  $915 \text{ cm}^{-1}$ . The band at about  $1,080 \text{ cm}^{-1}$  is due to the stretching vibration of the Si-O. The bands at  $525$  and  $466 \text{ cm}^{-1}$  are attributed to the stretching vibrations of Si-O-Al and bending vibrations, respectively [34,35]. For PASP, the bands at  $3,360$  and  $3,080 \text{ cm}^{-1}$  belong to N-H stretching vibration in

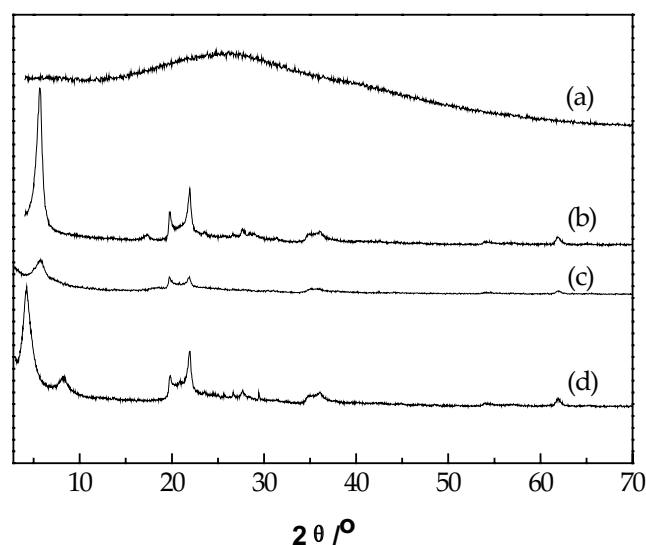


Fig. 1. XRD patterns of PASP (a), Mt (b), amino-Mt (c), and PASP/Mt (d).

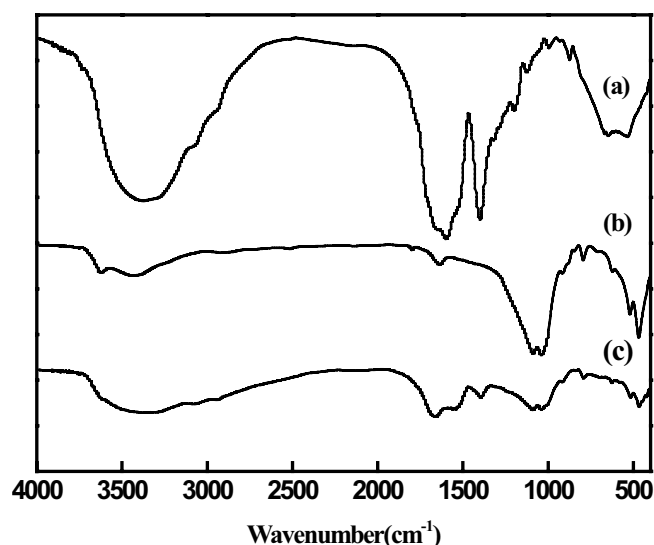


Fig. 2. FTIR spectra of PASP (a), Mt (b), and PASP/Mt (c).

–CONH and the band at  $1,654$  represents C–N stretching vibration in –CONH. The bands at  $1,600$  and  $1,390 \text{ cm}^{-1}$  are attributed to the coupling vibration and bending vibrations of C=O bonds in –CONH [36]. For PASP/Mt, the absorption bands showed both the characteristic vibrations of PASP and Mt. So it also presented that PASP was successfully grafted on the Mt.

The thermal behaviors of Mt, amino-Mt, and PASP/Mt are shown in Fig. 3. From Fig. 3, there were two important weight loss for Mt like  $25^\circ\text{C}$ – $160^\circ\text{C}$ , which is attributed to the removal of the interlayer water, and  $510^\circ\text{C}$ – $700^\circ\text{C}$ , which is due to the dehydration of hydroxyl groups along with the destruction of structure. While, the thermogravimetry of amino-Mt and PASP/Mt showed three stages weight loss. The first weight loss from about  $25^\circ\text{C}$  to  $140^\circ\text{C}$  should

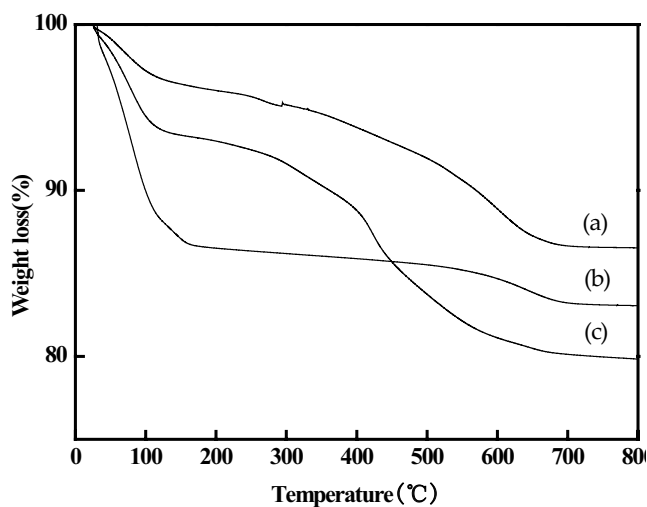


Fig. 3. TG analysis of amino-Mt (a), Mt (b), and PASP/Mt (c).

be ascribed to the removal of the interlayer water. The third weight loss from about 400°C to 700°C for PASP/Mt and from about 480°C to 700°C for amino-Mt is due to the removal of structural hydroxyl groups. It was also obvious that there existed the second weight loss district from about 210°C to 400°C for PASP/Mt and from about 210°C to 470°C for amino-Mt, which should be ascribed to the removal of PASP and amino groups. In addition, the weight loss PASP/Mt obviously increased comparison with the amino-Mt and Mt. It further presented that PASP was grafted on the surface of Mt.

### 3.2. Adsorption performance of PASP/Mt

#### 3.2.1. Effect of adsorbent amount

Fig. 4 shows the removal of Cu(II), Zn(II), and Ni(II) ions by PASP/Mt and Mt at different adsorbent amount. From Fig. 4 it is obvious that the removal percentages of Cu(II), Zn(II), and Ni(II) ions increased with the increase of adsorbent amount and the removal percentages of three metals by PASP/Mt were all higher than that of Mt, presenting that adsorption capacity of Mt was improved by grafting of PASP. So the amount of PASP/Mt should be 4 g L<sup>-1</sup> for the adsorption of Cu(II) and Zn(II), and the amount of PASP/Mt should be 12 g L<sup>-1</sup> for the adsorption of Ni(II).

#### 3.2.2. Effect of pH

The pH can significantly affect the adsorption process through changing the surface charge and protonation degree of functional groups on the active sites [37,38]. The effects of pH on the adsorption of Cu(II), Zn(II), and Ni(II) ions onto PASP/Mt are shown in Fig. 5. Because the hydroxide compounds would be produced as pH was over 7, so pH was varied from 1 to 7. The results showed that with the increase of pH from 1.0 to 6.0, the removal percentage increased significantly from 28% to 97% for Cu(II), 19% to 94% for Zn(II), and 16% to 96% for Ni(II). Then the removal percentage of the three metals was almost unchanged from

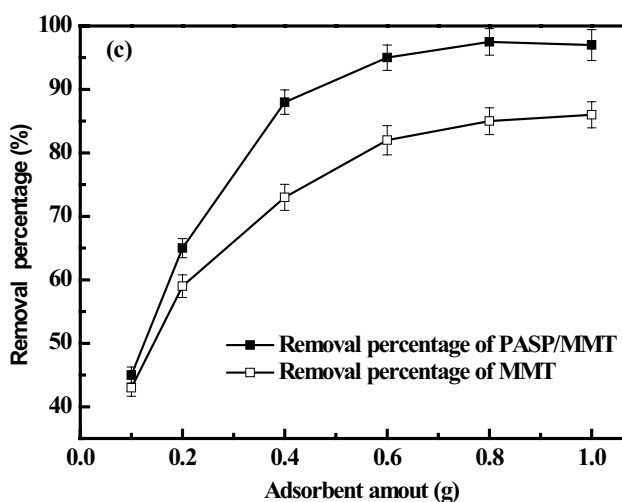
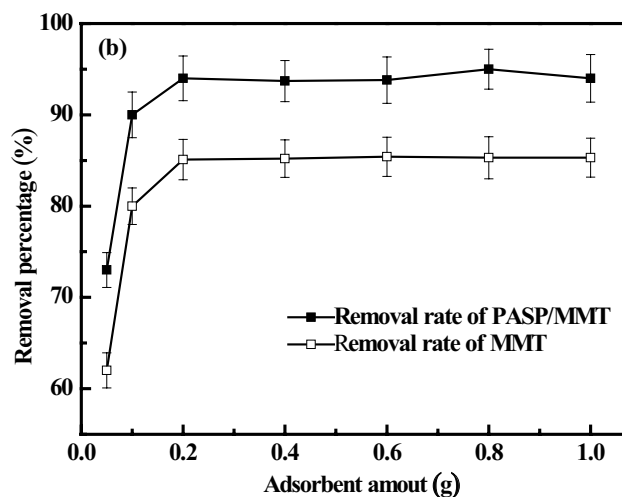
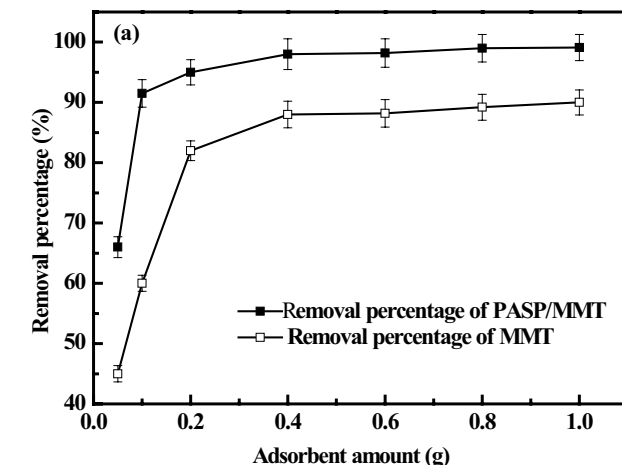


Fig. 4. The effect of adsorbent amount on the removal of Cu<sup>2+</sup> (a), Zn<sup>2+</sup> (b), and Ni<sup>2+</sup> (c).

pH = 6.0 to 7.0. At acidic solution, the carboxyl groups (–COOH) and amido bonds (–CO–NH–) of PASP was protonated and became the positively charged groups (–COOH<sub>2</sub><sup>+</sup>, –NH<sub>2</sub><sup>+</sup>). There existed the electrostatic repulsion forces between the positively charged groups and the

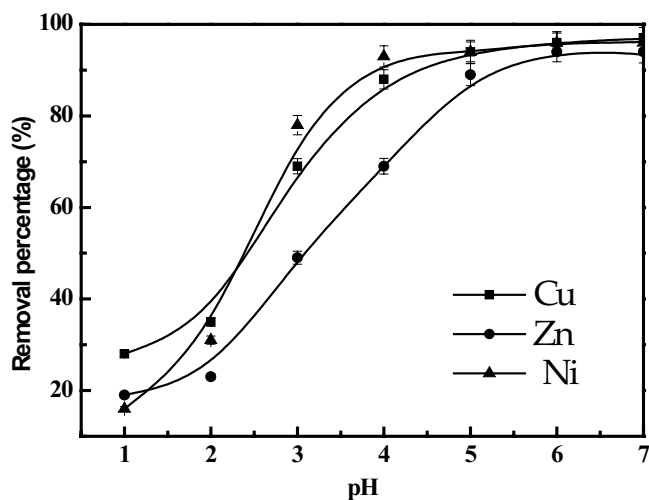


Fig. 5. Effect of pH on the adsorption of Cu(II), Zn(II), and Ni(II) ions onto PASP/Mt.

positively charged heavy metal ions, which would inhibit adsorption onto the adsorbent surface. In addition, there existed more  $H^+$  ions in lower pH medium of 1–3, which would provide a competition for the adsorption of the heavy metals and  $H^+$  onto the functional groups. Therefore, the optimum pH should be 5.5 for Cu(II), 6.0 for Zn(II), and 5.0 for Ni(II), respectively.

### 3.2.3. Adsorption kinetics

The relationships of contact time and adsorption capacity are performed in Fig. 6. Kinetic behavior was studied at four different concentrations by adsorption of Cu(II), Zn(II), and Ni(II) ions. From Fig. 6, it could be found that the removal of three metal ions onto PASP/Mt was rapid initially and then slowed down gradually. Finally, it was almost unchanged after about 20 min. Therefore, the equilibrium contact time could be at 20 min.

The kinetics of adsorption was analyzed by two kinetic models: first-order Lagergren model and second-order Lagergren model [39,40]. Both the two kinetic equations were used to describe the experimental data. The first-order Lagergren model can be depicted as follows:

$$\frac{dQ_t}{dt} = k_1(Q_e - Q_t) \quad (2)$$

The equation can be expressed in linear forms as follows:

$$\log(Q_e - Q_t) = \log(Q_e) - \frac{k_1 t}{2.303} \quad (3)$$

where  $Q_e$  and  $Q_t$  are the amounts of metal ions adsorbed at equilibrium and at time  $t$  ( $mg\ g^{-1}$ ) and  $k_1$  is the rate constant of first order adsorption ( $min^{-1}$ ). The plot of  $\log(Q_e - Q_t)$  versus  $t$  (not shown) should give the linear relationship from which  $k_1$  and  $Q_e$  can be determined by the slope and intercept, respectively. Parameters for the first-order model are summarized in Table 1.

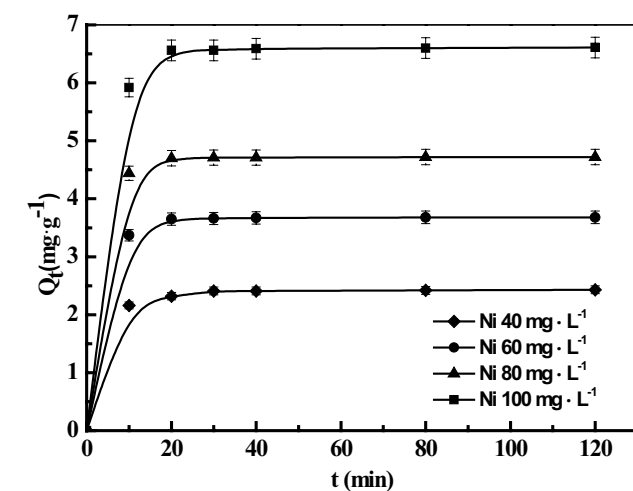
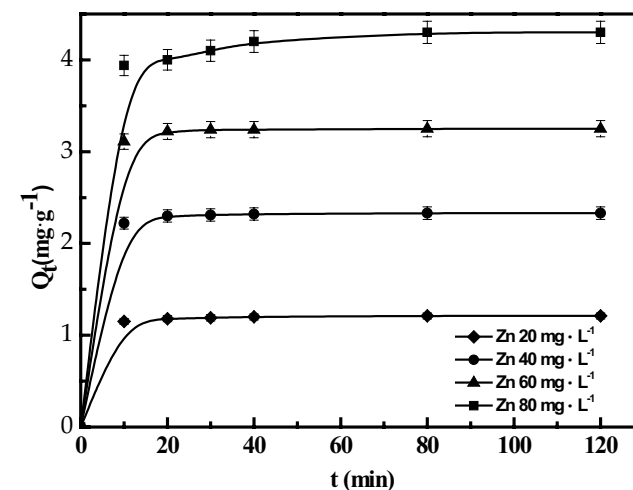
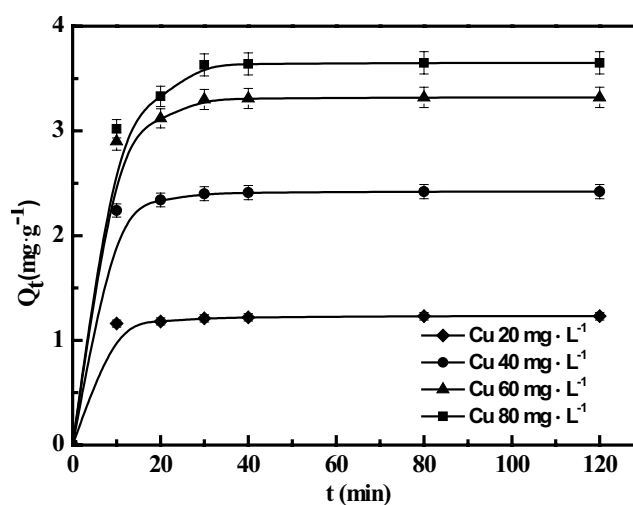


Fig. 6. Effect of contact time for the adsorption of Cu(II), Zn(II), and Ni(II) onto PASP/Mt at various initial concentrations.

Table 1  
Kinetic parameters for the adsorption of metal ions on PASP/Mt

Metal ions	Concentration (mg L <sup>-1</sup> )	First-order adsorption				Second-order adsorption		
		Q <sub>e</sub> (mg g <sup>-1</sup> ) (exp)	Q <sub>e</sub> (mg g <sup>-1</sup> ) (cal)	k <sub>1</sub> × 10 <sup>-2</sup> min <sup>-1</sup>	R <sup>2</sup>	Q <sub>e</sub> (mg g <sup>-1</sup> ) (cal)	k <sub>2</sub> × 10 <sup>-2</sup> min mg <sup>-1</sup>	R <sup>2</sup>
Cu <sup>2+</sup>	20	1.23	1.22	0.079	0.728	1.24	2.659	0.9999
	40	2.42	1.58	0.099	0.718	2.45	15.794	0.9999
	60	3.32	1.74	0.095	0.751	3.42	23.226	0.9994
	80	3.65	2.43	0.124	0.881	3.81	21.967	0.9986
Zn <sup>2+</sup>	20	1.21	1.20	0.150	0.878	1.22	3.079	0.9999
	40	2.33	2.00	0.170	0.866	2.35	23.700	0.9999
	60	3.25	2.39	0.185	0.854	3.28	70.928	0.9999
	80	4.3	2.57	0.080	0.590	4.31	74.886	0.9994
Ni <sup>2+</sup>	40	2.43	1.56	0.099	0.735	2.48	10.748	0.9997
	60	3.68	2.64	0.187	0.889	3.75	52.886	0.9995
	80	4.72	2.81	1.893	0.869	4.79	160.921	0.9997
	100	6.61	3.95	0.174	0.890	6.77	248.902	0.9991

The second-order Lagergren model can be expressed as follows:

$$\frac{dQ_t}{dt} = k_2(Q_e - Q_t)^2 \quad (4)$$

The equation can also be expressed in linear forms as follows:

$$\frac{t}{Q_t} = \frac{1}{k_2 Q_e^2} + \frac{t}{Q_e} \quad (5)$$

where  $Q_e$  and  $Q_t$  are the amounts of metal ions adsorbed at equilibrium and at time  $t$  (mg g<sup>-1</sup>) and  $k_2$  is the rate constant of second-order adsorption (min<sup>-1</sup>). The equilibrium adsorption capacity,  $Q_e$  and  $k_2$  were determined from the slope and the plot of  $t/Q_t$  versus  $t$  (Fig. 7) and parameters for the second-order model are summarized in Table 1.

According to Table 1, it was obvious that the correlation coefficients ( $R^2$ ) for the second-order model are all above 0.999 and  $R^2$  for the first-order model is lower than the second-order model. This presented that the second-order kinetics fits better for the adsorption of metal ions on PASP/Mt.

### 3.2.4. Adsorption isotherm

The equilibrium adsorption isotherm is the important data to understand the mechanism of the adsorption systems. So, in the work, the isotherm data for adsorption of metal ions on PASP/Mt was fitted by Langmuir, Freundlich, Dubinin–Radushkevich (D-R), and Temkin models [40]. The Freundlich model is an empirical equation, while the Langmuir isotherm is based on the assumption that all adsorption sites are identically homogeneous and the sorption of each sorbate molecule onto the surface has equal

sorption activation energy. The Langmuir and Freundlich isotherms can be expressed as follows:

$$\text{Langmuir } Q_e = \frac{bQ_m C_e}{1 + bC_e} \quad (6)$$

$$\text{Freundlich } Q_e = K_f C_e^n \quad (7)$$

The two equations can also be expressed in linear forms as follows:

$$\text{Langmuir } \frac{C_e}{Q_e} = \frac{1}{bQ_m} + \frac{C_e}{Q_m} \quad (8)$$

$$\text{Freundlich } \log Q_e = \log K_f + n \log C_e \quad (9)$$

where  $Q_e$  is the equilibrium metal ions per unit mass of the adsorbent (mg g<sup>-1</sup>),  $C_e$  is the equilibrium metal ions in the solution (mg L<sup>-1</sup>),  $Q_m$  is the maximum adsorption capacity (mg g<sup>-1</sup>),  $b$  is a sorption constant,  $K_f$  and  $n$  are empirical constants related to the sorption capacity and adsorption intensity.

D-R isotherm usually expresses the adsorption mechanism with a Gaussian energy distribution onto a heterogeneous surface. It can be expressed as follows:

$$Q_e = Q_s \exp(-B\varepsilon^2) \quad (10)$$

The linearized form of D-R isotherm is as follows:

$$\ln Q_e = \ln Q_s - 2BRT \ln \left[ 1 + \frac{1}{C_e} \right] \quad (11)$$

where  $Q_e$  is the equilibrium metal ions per unit mass of the adsorbent (mg g<sup>-1</sup>),  $Q_s$  is theoretical isotherm saturation capacity (mg g<sup>-1</sup>), and  $\varepsilon$  is D-R isotherm constant.

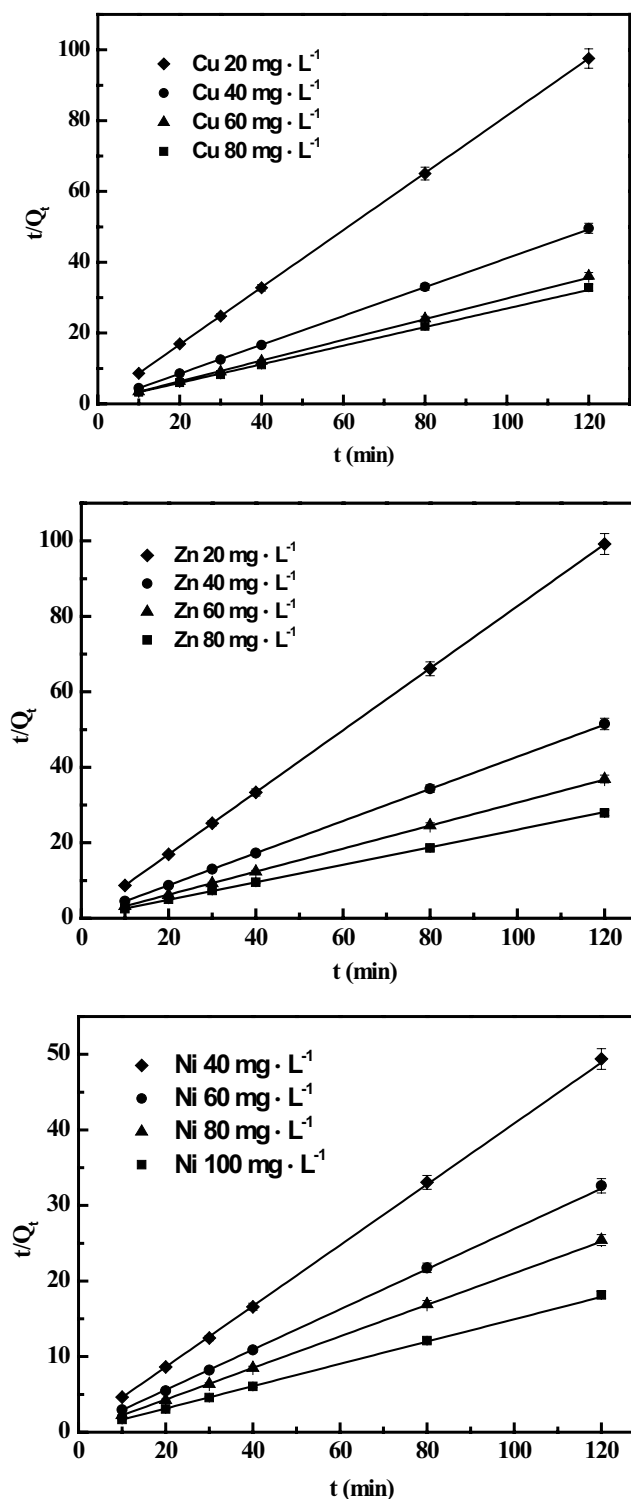


Fig. 7. Second-order kinetics model plots for adsorption of Cu(II), Zn(II), and Ni(II) onto PASP/Mt.

The constant  $B$  gives the mean free energy of adsorption per molecule of the sorbate when it is transferred from the solid from infinity in the solution and the relation is given as follows:

$$E = \left[ \frac{1}{\sqrt{2B}} \right] \quad (12)$$

The Temkin isotherm explains the interaction between the adsorbent and sorbate molecules. This isotherm is commonly used in the form of the following equation:

$$Q_e = \left( \frac{RT}{b} \right) \ln(AC_e) \quad (13)$$

The equation can also be expressed in linear forms as follows:

$$Q_e = B \ln A + B \ln C_e \quad (14)$$

where  $B = RT/b$ ,  $b$  is the Temkin constant related to heat of sorption ( $\text{J mol}^{-1}$ ), and  $A$  is the Temkin isotherm constant ( $\text{L g}^{-1}$ ).

Fig. 8 shows the adsorption isotherms of Cu(II), Zn(II), and Ni(II) ions with initial concentrations of  $20 \text{ mg L}^{-1}$  (Cu(II)),  $20 \text{ mg L}^{-1}$  (Zn(II)) and  $40 \text{ mg L}^{-1}$  (Ni(II)). The adsorption experimental data and its predicted values by Langmuir, Freundlich, D-R, and Temkin models are shown in Figs. 9–12, respectively. Constant parameters and correlation coefficient calculated for Langmuir, Freundlich, D-R, and Temkin isotherm models are summarized in Table 2. As seen in the figures and based on the  $R^2$  values, it was obvious that Freundlich model was much better than that of the other three models for the adsorption of Cu(II), Langmuir model was much better than that of the other three models for the adsorption of Ni(II), and Temkin model was much better than that of the other three models for the adsorption of Zn(II). Moreover, in here,  $n$  was all between 0 and 1, presenting a favorable adsorption.  $E$  could also be used to estimating the type of adsorption process. From Table 2, in this system they were 0.228, 0.4677, and 0.1036  $\text{kJ mol}^{-1}$ , which was smaller than the energy range of physical adsorption reaction (8–16  $\text{kJ mol}^{-1}$ ).

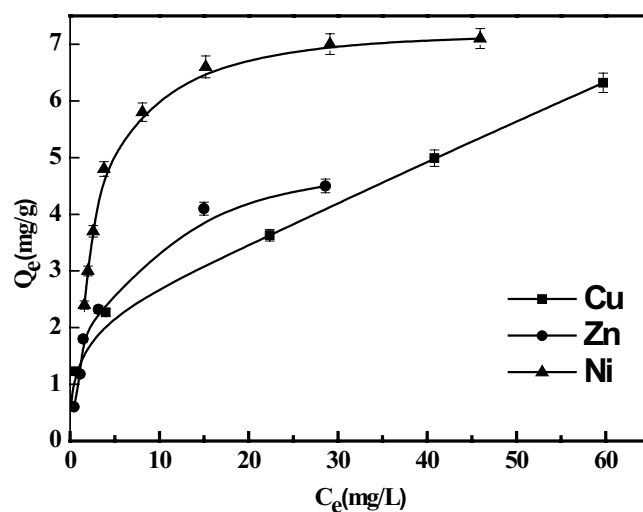


Fig. 8. Adsorption isotherm of Cu(II), Zn(II), and Ni(II) ions onto PASP/Mt.

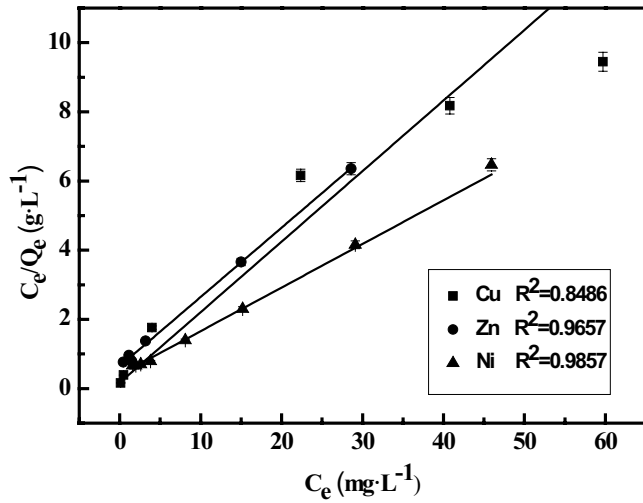


Fig. 9. Langmuir isotherm plots for adsorption of Cu(II), Zn(II), and Ni(II) onto PASP/Mt.

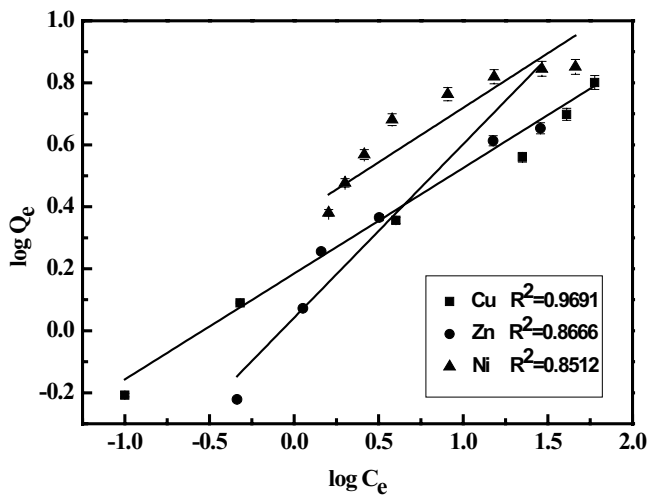


Fig. 10. Freundlich isotherm plots for adsorption of Cu(II), Zn(II), and Ni(II) onto PASP/Mt.

indicating that the adsorption of  $\text{Cu}^{2+}$ ,  $\text{Zn}^{2+}$ , and  $\text{Ni}^{2+}$  was physical adsorption. In addition, comparison of the adsorption capacity for Ni(II), Cu(II), and Zn(II) with different adsorbents (Table 3), the PASP/Mt was the effective adsorbent for metal ions, and could certainly be competitive with other adsorbents. Moreover, PASP is biodegradable and Mt is inexpensive in nature. Therefore, it is feasibility of using PASP/Mt as the adsorbent.

### 3.2.5. Thermodynamic studies

Thermodynamic experiments were conducted at the initial concentrations of  $20 \text{ mg L}^{-1}$  for Cu(II) and Zn(II),  $40 \text{ mg L}^{-1}$  for Ni(II) from  $20^\circ\text{C}$  to  $40^\circ\text{C}$ . The thermodynamic parameters can be presented by the following equations:

$$K_d = \frac{Q_e}{C_e} \quad (15)$$

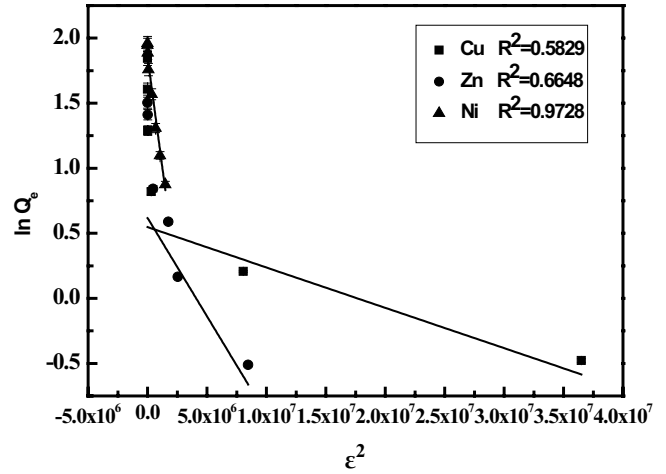


Fig. 11. Dubinin–Radushkevich isotherm plots for adsorption of Cu(II), Zn(II), and Ni(II) onto PASP/Mt.

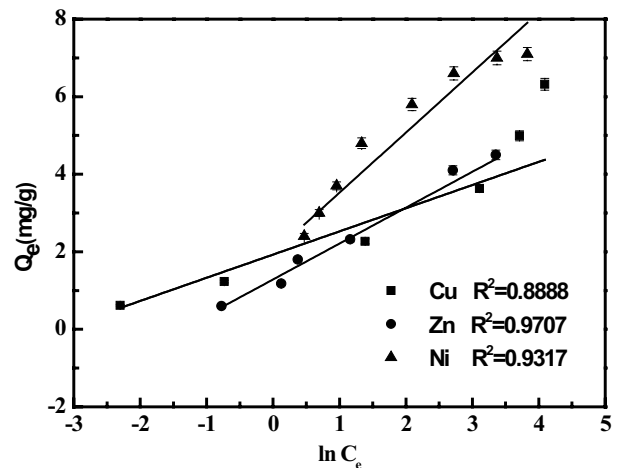


Fig. 12. Temkin isotherm plots for adsorption of Cu(II), Zn(II), and Ni(II) onto PASP/Mt.

$$\Delta G^\circ = -RT \ln K_d \quad (16)$$

$$\ln K_d = \frac{\Delta S^\circ}{R} - \frac{\Delta H^\circ}{RT} \quad (17)$$

where  $Q_e$  is the equilibrium metal ions per unit mass of the adsorbent ( $\text{mg g}^{-1}$ ),  $C_e$  is the equilibrium metal ions in the solution ( $\text{mg L}^{-1}$ ),  $R$  is the gas constant ( $8.314 \text{ J mol}^{-1} \text{ K}^{-1}$ ),  $K_d$  and  $T$  are equilibrium constant and temperature (K), enthalpy ( $\Delta H^\circ$ ) and entropy ( $\Delta S^\circ$ ) obtained from slope and intercept by plotting a straight line of  $\ln K_d$  versus  $1/T$ . Gibbs free energy ( $\Delta G^\circ$ ) was also calculated in Table 4.

Generally, the change of free energy for physisorption is between  $-20$  and  $0 \text{ kJ mol}^{-1}$ , and chemisorption is in a range of  $-80$  to  $-400 \text{ kJ mol}^{-1}$  [46]. According to Table 4, the positive change of the standard enthalpy ( $\Delta H^\circ$ ) indicated that the adsorption of Cu(II), Zn (II), and Ni(II) was an endothermic process. The positive change of standard entropy

Table 2  
Isotherm parameters for adsorption of Cu(II), Zn(II), and Ni(II) onto PASP/Mt

Isotherm	Constant			
	$Q_m$ (mg g <sup>-1</sup> )	$b$ (L mg <sup>-1</sup> )	$R_L$	$R^2$
Langmuir				
Cu(II)	4.9036	28.0894	0.0018	0.8486
Zn(II)	4.9913	7.7575	0.0064	0.9657
Ni(II)	7.9315	19.9124	0.0013	0.9857
Freundlich	$K_f$ (mg g <sup>-1</sup> )	$n$ (L mg <sup>-1</sup> )		$R^2$
Cu(II)	1.5286	0.3411		0.9692
Zn(II)	1.099	0.56		0.8666
Ni(II)	2.3281	0.351		0.8512
D-R	$Q_s$ (mol g <sup>-1</sup> )	$B_D$ (mol <sup>2</sup> K J <sup>-2</sup> )	$E$ (kJ mol <sup>-1</sup> )	$R^2$
Cu(II)	1.7289	3.1011	0.228	0.5829
Zn(II)	1.856	1.5119	0.4677	0.6648
Ni(II)	6.3912	6.8232	0.1036	0.9728
Temkin	$A$ (L g <sup>-1</sup> )		$B$ (J mol <sup>-1</sup> )	$R^2$
Cu(II)	25.1134		0.598	0.8888
Zn(II)	4.0217		0.9255	0.9707
Ni(II)	3.5723		1.5503	0.9317

Table 3  
Comparison of adsorption properties of metal ions on various adsorbents

Adsorbent	$Q_m$ (mg g <sup>-1</sup> )	Adsorbed metal ions	Ref.
Lignin (black liquor)	22.86	Cu <sup>2+</sup>	[41]
Lignin (black liquor)	11.25	Zn <sup>2+</sup>	
Lignin (black liquor)	5.99	Ni <sup>2+</sup>	
Activated carbon	18.68	Cu <sup>2+</sup>	[42]
Activated carbon	16.12	Ni <sup>2+</sup>	
Activated carbon	12.19	Zn <sup>2+</sup>	
Grafted chitin	6.4	Cu <sup>2+</sup>	[43]
Chitin-humic acid	5.83	Ni <sup>2+</sup>	[44]
Carboxylated chitin	5.14	Cu <sup>2+</sup>	[43]
Chitin (crab shells)	4.36	Ni <sup>2+</sup>	[44]
Protonated chitin	4.23	Cu <sup>2+</sup>	[43]
Kraft lignin	3.37	Cu <sup>2+</sup>	[45]
Kraft lignin	1.77	Zn <sup>2+</sup>	
PASP/Mt	6.61	Ni <sup>2+</sup>	This work
PASP/Mt	4.11	Zn <sup>2+</sup>	This work
PASP/Mt	3.64	Cu <sup>2+</sup>	This work

( $\Delta S^\circ$ ) values corresponded to an increase in the degree of freedom of the adsorbed species. The water molecules and conformational changes of PASP might be responsible for the positive entropy change. It was also found that the adsorption of Cu(II) and Ni(II) was a spontaneous process in the tested temperature and there was the physisorption on the surface of adsorbent.

Table 4  
Thermodynamic parameters for adsorption of Cu(II), Zn(II), and Ni(II) onto PASP/Mt

Metal ion	$T$ (K)	$\Delta G^\circ$	$\Delta H^\circ$	$\Delta S^\circ$
		kJ mol <sup>-1</sup>	kJ mol <sup>-1</sup>	J mol <sup>-1</sup> K <sup>-1</sup>
Cu(II)	293.15	-1.27	25.84	90.57
	303.15	-1.84		
	313.15	-2.19		
Zn(II)	293.15	1.46	20.00	62.74
	303.15	0.53		
	313.15	0.68		
Ni(II)	293.15	-0.97	11.31	41.56
	303.15	-1.37		
	313.15	-1.61		

### 3.2.6. Selectivity in a binary-metal system

The binary-metal adsorption of Cu(II), Zn(II), and Ni(II) was conducted to investigate the preferential adsorption on PASP/Mt composite. The results are shown in Fig. 13. From Fig. 13, Cu(II) was preferentially adsorbed over Zn(II), and Ni(II) in the binary-metal system and the selectivity of PASP/Mt for the metals was arranged in the following sequence: Cu(II) > Zn(II) > Ni(II). It was also interesting that the removal percentage of Ni(II) greatly decreased in the binary-metal system. The relative affinity of metal ions onto PASP/Mt should be associated with properties such as electronegativity, hydrolysis constant, and hydrated ionic radius (Table 5). The preference for Cu(II) might be ascribed to the high electronegativity, small hydrolysis constant, and hydrated ionic radius [38,47]. According to the characterization results and adsorption isotherm, there were abundant carboxyl groups (-COOH) and amido bonds (-CO-NH-) on the surface of the adsorbent, and the adsorption of Cu(II) onto PASP/Mt fits better with the Freundlich model. So, it could be reasonably

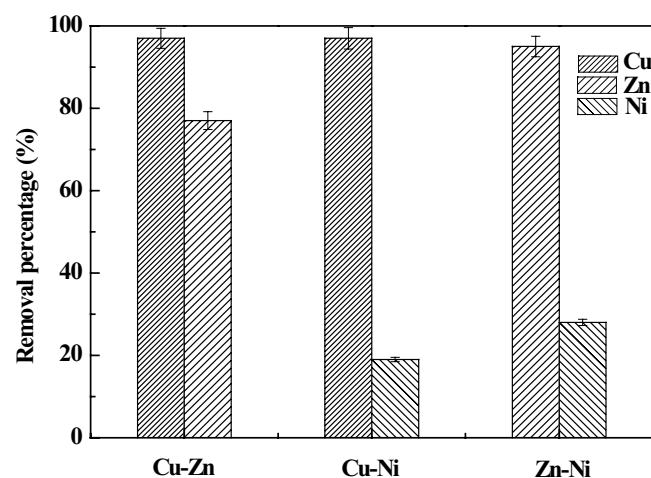


Fig. 13. Behavior of Cu(II), Zn(II), and Ni(II) removal in the binary-metal system.

Table 5  
Physical properties of Cu(II), Zn(II), and Ni(II) [38]

Parameters	Cu(II)	Zn(II)	Ni(II)
Hydrated ionic radius (Å)	4.19	4.30	4.04
Hydrolysis constant ( $PK_1$ )	8.0	9.0	9.9
Electronegativity	1.95	1.6	1.91

suggested that there existed the stronger attraction between Cu(II) and the adsorbent than other metals and the highest electronegativity of Cu(II) should be the critical factor for the adsorption.

#### 4. Conclusions

In this work, PASP-grafted Mt was prepared and characterized by FTIR, XRD, and TG. The characterization results showed that PASP was successfully grafted on the surface of Mt. The adsorption results showed that adsorption capacity of Mt was improved by grafting of PASP for the removal of Cu(II), Zn(II), and Ni(II) ions from aqueous solution. pH was an important factor and the optimum pH was 5.5 for Cu(II), 6.0 for Zn(II), and 5.0 for Ni(II), respectively. The kinetics experiments revealed that the second-order model represented the experimental kinetic data in a better manner than first-order model. It was found that the adsorption isotherm of Cu(II) onto PASP/Mt fits better with the Freundlich model, while Zn(II) and Ni(II) ions adsorption belongs to Temkin and Langmuir models, respectively. The selectivity of PASP/Mt for the metals in a binary system was as the following sequence: Cu(II) > Zn(II) > Ni(II). So PASP-grafted Mt is the efficient catalyst for the adsorption of metal ions and it may be the alternative substitute to the more costly adsorbents such as activated carbon.

#### Acknowledgments

The authors wish to acknowledge the Natural Scientific Foundation of Zhejiang Province ZJNSF (LY16B030010), the financial support from the National Natural Scientific Foundation of China (21506188), China Postdoctoral Science Foundation (2018M630688) and Project of Zhejiang “151” talents project.

#### References

- [1] S.Y. Kim, S. Parambadath, S.S. Park, C.S. Ha, Melamine-sulfonic acid functionalized SBA-15 for selective adsorption of metal ions from artificial seawater and wastewater, *J. Nanosci. Nanotechnol.*, 17 (2017) 7565–7574.
- [2] S. Vasudevan, J. Lakshmi, G. Sozhan, Electrocoagulation studies on the removal of copper from water using mild steel electrode, *Water Environ. Res.*, 84 (2012) 209–219.
- [3] W. Yao, J. Wang, P.Y. Wang, X.X. Wang, S.J. Yu, Y.D. Zou, J. Hou, T. Hayat, A. Alsaedi, X.K. Wang, Synergistic coagulation of GO and secondary adsorption of heavy metal ions on Ca/Al layered double hydroxides, *Environ. Pollut.*, 229 (2017) 827–836.
- [4] Y.N. Chen, W. Zhao, J.C. Zhang, Preparation of 4-vinylpyridine (4VP) resin and its adsorption performance for heavy metal ions, *RSC Adv.*, 7 (2017) 4226–4236.
- [5] S. Vasudevan, J. Lakshmi, Process conditions and kinetics for the removal of copper from water by electrocoagulation, *Environ. Eng. Sci.*, 29 (2012) 563–572.
- [6] T.J. Afolabi, A.O. Alade, M.O. Jimoh, I.O. Fashola, Heavy metal ions adsorption from dairy industrial wastewater using activated carbon from milk bush kernel shell, *Desal. Wat. Treat.*, 57 (2016) 14565–14577.
- [7] S. Vasudevan, J. Lakshmi, G. Sozhan, Optimization of electrocoagulation process for the simultaneous removal of mercury, lead, and nickel from contaminated water, *Environ. Sci. Pollut. Res.*, 19 (2012) 2734–2744.
- [8] S. Vasudevan, J. Lakshmi, R. Kamaraj, G. Sozhan, A critical study on the removal of copper by an electrochemically assisted coagulation: equilibrium, kinetics, and thermodynamics, *Asia Pac. J. Chem. Eng.*, 8 (2013) 162–171.
- [9] P. Chanpiwat, S. Sthiannopkao, K. Widmer, S. Himeno, H. Miyataka, N.U. Vu, V.V. Tran, T.T.N. Pham, Assessment of metal and bacterial contamination in cultivated fish and impact on human health for residents living in the Mekong Delta, *Chemosphere*, 163 (2016) 342–350.
- [10] G. Plavan, O. Jitar, C. Teodosiu, M. Nicoara, D. Micu, S.A. Strungaru, Toxic metals in tissues of fishes from the Black Sea and associated human health risk exposure, *Environ. Sci. Pollut. Res. Int.*, 24 (2017) 7776–7787.
- [11] R.A. Root, S.M. Hayes, C.M. Hammond, R.M. Maier, J. Chorover, Toxic metal(loid) speciation during weathering of iron sulfide mine tailings under semi-arid climate, *Appl. Geochem.*, 62 (2015) 131–149.
- [12] Y. Shandil, U.K. Dautoo, G.S. Chauhan, New modified poly(vinylamine)-gels as selective and efficient  $Hg^{2+}$  ions adsorbents, *Chem. Eng. J.*, 316 (2017) 978–987.
- [13] K. Anbalagan, P.S. Kumar, R. Karthikeyan, Adsorption of toxic Cr(VI) ions from aqueous solution by sulphuric acid modified *Strychnos potatorum* seeds in batch and column studies, *Desal. Wat. Treat.*, 57 (2016) 12585–12607.
- [14] S.S. Madaeni, E. Salehi, Adsorption of cations on nanofiltration membrane: separation mechanism, isotherm confirmation and thermodynamic analysis, *Chem. Eng. J.*, 150 (2009) 114–121.
- [15] G.V. Mejia, V. Martinez-Miranda, C. Fall, I. Linares-Hernandez, M. Solache-Rios, Comparison of Fe-Al-modified natural materials by an electrochemical method and chemical precipitation for the adsorption of F- and As(V), *Environ. Technol.*, 37 (2016) 558–568.
- [16] S. Maleki, A. Karimi-Jashni, Effect of ball milling process on the structure of local clay and its adsorption performance for Ni(II) removal, *Appl. Clay Sci.*, 137 (2017) 213–224.
- [17] C. Hu, P.F. Zhu, M. Cai, H.Q. Hu, Q.L. Fu, Comparative adsorption of Pb(II), Cu(II) and Cd(II) on chitosan saturated montmorillonite: kinetic, thermodynamic and equilibrium studies, *Appl. Clay Sci.*, 143 (2017) 320–326.
- [18] E.D. Freitas, A.C.R. Carmo, A.F.A. Neto, M.G.A. Vieira, Binary adsorption of silver and copper on Verde-Iodo bentonite: kinetic and equilibrium study, *Appl. Clay Sci.*, 137 (2017) 69–76.
- [19] U.K. Sahu, S. Sahu, S.S. Mahapatra, R.K. Patel, Cigarette soot activated carbon modified with Fe(3)o(4) nanoparticles as an effective adsorbent for As(III) and As(V): material preparation, characterization and adsorption mechanism study, *J. Mol. Liq.*, 243 (2017) 395–405.
- [20] A.M. Youssef, A.I. Ahmed, M.I. Amin, U.A. El-Banna, Adsorption of lead by activated carbon developed from rice husk, *Desal. Wat. Treat.*, 54 (2015) 1694–1707.
- [21] D. Zhang, C.H. Zhou, C.X. Lin, D.S. Tong, W.H. Yu, Synthesis of clay minerals, *Appl. Clay Sci.*, 50 (2010) 1–11.
- [22] L.M. Wu, C.H. Zhou, J. Keeling, D.S. Tong, W.H. Yu, Towards an understanding of the role of clay minerals in crude oil formation, migration and accumulation, *Earth Sci. Rev.*, 115 (2012) 373–386.
- [23] A.A.M. Abdel-Karim, W. Elwan, M.R. El-Naggar, M.M. Gouda, Experimental and modeling investigations of cesium and strontium adsorption onto clay of radioactive waste disposal, *Appl. Clay Sci.*, 132 (2016) 391–401.
- [24] Y. Bentahar, C. Hurel, K. Draoui, S. Khairoun, N. Marmier, Adsorptive properties of Moroccan clays for the removal of arsenic(V) from aqueous solution, *Appl. Clay Sci.*, 119 (2016) 385–392.
- [25] M. Fouodjouo, H. Fotouo-Nkaffo, S. Laminsi, F.A. Cassini, L.O. Brito-Benetoli, N.A. Debacher, Adsorption of copper (II)

- onto cameroonian clay modified by non-thermal plasma: characterization, chemical equilibrium and thermodynamic studies, *Appl. Clay Sci.*, 142 (2017) 136–144.
- [26] K.E. Adraa, T. Georgelin, J.F. Lambert, F. Jaber, F. Tielens, M. Jaber, Cysteine-montmorillonite composites for heavy metal cation complexation: a combined experimental and theoretical study, *Chem. Eng. J.*, 314 (2017) 406–417.
- [27] H.P. He, Q. Tao, J.X. Zhu, P. Yuan, W. Shen, S.Q. Yang, Silylation of clay mineral surfaces, *Appl. Clay Sci.*, 71 (2013) 15–20.
- [28] I. Ostolska, M. Wisniewska, Comparison of the influence of polyaspartic acid and polylysine functional groups on the adsorption at the  $\text{Cr}_2\text{O}_3$  – aqueous polymer solution interface, *Appl. Surf. Sci.*, 311 (2014) 734–739.
- [29] J.X. Chen, L.H. Xu, J. Han, M. Su, Q. Wu, Synthesis of modified polyaspartic acid and evaluation of its scale inhibition and dispersion capacity, *Desalination*, 358 (2015) 42–48.
- [30] S. Sharma, A. Dua, A. Malik, Polyaspartic acid based superabsorbent polymers, *Eur. Polym. J.*, 59 (2014) 363–376.
- [31] G.F. Ma, Q. Yang, F.T. Ran, Z.B. Dong, Z.Q. Lei, High performance and low cost composite superabsorbent based on polyaspartic acid and palygorskite clay, *Appl. Clay Sci.*, 118 (2015) 21–28.
- [32] S.J. Chipera, D.L. Bish, Baseline studies of the clay minerals society source clays: powder X-ray diffraction analyses, *Clay Clay Miner.*, 49 (2001) 398–409.
- [33] A. Viani, A.F. Gualtieri, A.G. Gualtieri, The nature of disorder in montmorillonite by simulation of X-ray powder patterns, *Am. Mineral.*, 87 (2002) 966–975.
- [34] J. Madejova, P. Komadel, Baseline studies of the clay minerals society source clays: infrared methods, *Clay Clay Miner.*, 49 (2001) 410–432.
- [35] P. Djomgoue, D. Njopwouo, FT-IR spectroscopy applied for surface clays characterization, *J. Surf. Eng. Mater. Adv. Technol.*, 3 (2013) 275–282.
- [36] A. Vegotsky, K. Harada, S.W. Fox, The characterization of polyaspartic acid and some related compounds, *J. Am. Chem. Soc.*, 80 (1958) 3361–3366.
- [37] A.S. Ozcan, B. Erdem, A. Ozcan, Adsorption of Acid Blue 193 from aqueous solutions onto BTMA-bentonite, *Colloids Surf., A*, 266 (2005) 73–81.
- [38] W.C. Tsai, I.B. Sonia, C.C. Kan, C.M. Futalan, M.L.P. Dalida, M.W. Wan, Removal of copper, nickel, lead, and zinc using chitosan-coated montmorillonite beads in single- and multi-metal system, *Desal. Wat. Treat.*, 57 (2015) 1–14.
- [39] R. Kamaraj, P. Ganesan, S. Vasudevan, Removal of lead from aqueous solutions by electrocoagulation: isotherm, kinetics and thermodynamic studies, *Int. J. Environ. Sci. Technol.*, 12 (2015) 683–692.
- [40] R. Kamaraj, A. Pandiarajan, S. Jayakiruba, M. Naushad, S. Vasudevan, Kinetics, thermodynamics and isotherm modeling for removal of nitrate from liquids by facile one-pot electrosynthesized nano zinc hydroxide, *J. Mol. Liq.*, 215 (2016) 204–211.
- [41] X. Guo, S. Zhang, X. Shan, Adsorption of metal ions on lignin, *J. Hazard. Mater.*, 151 (2008) 134–142.
- [42] F. Bouhamed, Z. Elouear, J. Bouzid, B. Ouddane, Multi-component adsorption of copper, nickel and zinc from aqueous solutions onto activated carbon prepared from date stones, *Environ. Sci. Pollut. Res.*, 23 (2016) 1–6.
- [43] G.N. Kousalya, M.R. Gandhi, N. Viswanathan, S. Meenakshi, Preparation and metal uptake studies of modified forms of chitin, *Int. J. Biol. Macromol.*, 47 (2010) 583–589.
- [44] S.J. Santosa, D. Siswanta, A. Kurniawan, W.H. Rahmanto, Hybrid of chitin and humic acid as high performance sorbent for Ni(II), *Surf. Sci.*, 601 (2007) 5155–5161.
- [45] M.B. Šćiban, M.T. Klasnja, M.G. Antov, Study of the biosorption of different heavy metal ions onto Kraft lignin, *Ecol. Eng.*, 37 (2011) 2092–2095.
- [46] M.J. Jaycock, G.D. Parfitt, *Chemistry of Interfaces*, E. Horwood, Hoboken, New Jersey, USA, 1981.
- [47] S.M. Musyoka, H. Mittal, S.B. Mishra, J.C. Ngila, Effect of functionalization on the adsorption capacity of cellulose for the removal of methyl violet, *Int. J. Biol. Macromol.*, 65 (2014) 389–397.